Open Ceramics 1 (2020) 100001

Contents lists available at ScienceDirect

Open Ceramics

journal homepage: www.editorialmanager.com/oceram

Metal-containing ceramic nanocomposites synthesized from metal acetates and polysilazane

Jun Wang [a], Valérie Schölch [a], Oliver Görke [a], Götz Schuck [b], Xifan Wang [a], Gaofeng Shao [a], Susan Schorr [b,c], Maged F. Bekheet [a,*], Aleksander Gurlo [a]

[a] Fachgebiet Keramische Werkstoffe / Chair of Advanced Ceramic Materials, Institut für Werkstoffwissenschaften und-technologien, Technische Universität Berlin, Hardenbergstraße 40, 10623, Berlin, Germany
[b] Helmholtz-Zentrum Berlin für Materialien und Energie, Hahn-Meitner-Platz 1, 14109, Berlin, Germany
[c] Free University Berlin, Department of Geosciences, Malteserstraße 74-100, 12249, Berlin, Germany

ARTICLE INFO

Keywords:
Poly(vinyl)silazane
Metal acetates
Metal-containing precursors
Polymer-derived ceramics
Metal
Metal silicide
Nanocomposites

ABSTRACT

Metal-containing (Mn, Fe, Co, Cu, Zn and Ag) polysilazane precursors are synthesized via one-step chemical reaction of metal acetates with poly(vinyl)silazane (Durazane 1800) at room temperature under argon atmosphere. The ATR-FTIR spectra of the synthesized metal-containing precursors reveal that the metal acetates used in the synthesis catalyze the hydrosilylation reaction between -Si-H and -Si-CH═CH_2 groups in polysilazane. The XPS and XRD characterizations indicate that the metallic phase is directly generated in precursors after the reaction of Durazane 1800 polymer with $Fe(CH_3COO)_2$, $Co(CH_3COO)_2{\cdot}4H_2O$, $CuCH_3COO$, $Cu(CH_3COO)_2$, $AgCH_3COO$. Ceramic nanocomposites containing either metal or metal silicide are obtained after the pyrolysis of the synthesized metal-containing precursors at 700 °C and 1100 °C under argon atmosphere.

1. Introduction

Silicon-containing polymer-derived ceramics (PDCs) are promising candidates for a wide range of high-temperature applications due to their higher thermal stability, good corrosion and oxidation resistance, as well as excellent thermomechanical properties [1–3]. Si-containing PDCs can be synthesized as nanocomposites by varying architecture or chemical composition of preceramic precursors [4]. Among them, metal-containing PDCs nanocomposites are of great interest in engineering fields due to their magnetic, electrical and catalytic properties [5–8].

Metal-containing PDCs nanocomposites are usually synthesized via active fillers control pyrolysis (AFCOP) process by the direct blending of preceramic precursors with active fillers of metal powders such as Ti [9], Cr [10], Fe [11], and Ni [12] or metal oxides such as Fe_3O_4 [13], ZnO [14], and TiO_2 [15]. These active fillers can reduce the shrinkage and porosity generation of the ceramic nanocomposites during the pyrolysis process. Thus, AFCOP can be considered as a near-net-shape technique to provide the possibility to produce large-size and fully densified polymer-derived ceramic parts. Moreover, the obtained ceramic nanocomposites may exhibit improved thermochemical and functional properties compared with pure phases [16–19]. However, active fillers are limited with their particle size and heterogeneous morphology. The dispersed filler particles are usually observed in the ceramic matrix due to the insolubility of inorganic powders in organic solvent used in the synthesis [13,20].

Therefore, attention has been directed towards molecular pathways such as the pyrolysis of organometallic polymers containing both organosilicon and metals in their structure [21–24]. Organometallic complexes usually can be pyrolyzed at relatively low temperature 400–600 °C, which will lead to the formation of metal clusters homogeneously dispersed in ceramic matrix. Indeed, the dispersion of metal at the atomic level in the polymer precursors can help in the control of both the stoichiometry and microstructure of the derived ceramics. For instance, a ferromagnetic ceramic composites containing iron, silicon, carbon elements were synthesized through the thermal decomposition of poly(-ferrocenylsilanes) [25]. However, this synthesis approach is limited by the restricted variety of available precursors. The more general molecular approach is to use organometallic compounds such as iron and cobalt carbonyls [26–29], which are extremely toxic and easily vaporize during the ceramization process at high temperature. Metal alkoxides such as aluminium isopropoxide or early transition metal alkoxides, for example,

* Corresponding author.
E-mail address: maged.bekheet@ceramics.tu-berlin.de (M.F. Bekheet).

https://doi.org/10.1016/j.oceram.2020.100001
Received 11 February 2020; Received in revised form 8 April 2020; Accepted 8 April 2020
Available online 16 April 2020

titanium n-propoxide and hafnium n-butoxide, have shown the potential to interact with polymer precursors to form Si–O-M units with the evolution of alkanes [30–33]. However, for the late transition metals (such as Co, Cu and Pd) that would be very interesting for catalysts, the corresponding metal alkoxides are not available. Recently, we reported the in situ formation of Ni nanoparticles in nanoporous silicon oxycarbonitride ceramic matrix via a chemical reaction of polysilazane HTT1800 polymer with trans-[bis(2-aminoetanol-N,O) diacetato-nickel(II)] single crystals [34]. Similarly, a molecular approach for the modification of polysilazane HTT1800 with aminopyridinato metal complexes was developed to introduce several transition metals (*e.g.* Fe, Cu, Ni, Pt, Pd) into PDCs matrix [35–38]. However, despite trans-[bis(2-aminoetanol-N,O)diacetato-nickel(II)] single crystals and aminopyridinato metal complexes can be synthesized in good yield and are also soluble in most organic solvents, but their synthesis is complicated and time-consuming.

In this work, we report a one-step chemical approach to synthesize metal-containing polysilazane precursors via the reaction of metal acetates with poly(vinyl)silazane (Durazane 1800). This chemical modification approach is advantageous, owing to the very simple reaction condition (in an ice bath under argon atmosphere), the use of rather inexpensive poly(vinyl)silazane (Durazane 1800) and easily accessible commercial metal acetate materials. The obtained metal-containing polysilazane precursors as well as their derived ceramic nanocomposites after pyrolyzing at 700 °C and 1100 °C under argon atmosphere are characterized using several techniques such as ATR-FTIR, XPS, XANES, STA-MS and XRD.

2. Experimental section

2.1. Materials

Metal acetates - $Mg(CH_3COO)_2{\cdot}4H_2O$ (98%), $Mn(CH_3COO)_2{\cdot}4H_2O$ (99%), $Mn(CH_3COO)_3{\cdot}2H_2O$ (97%), $Mn(CH_3COO)_2$ (98%), $Fe(CH_3COO)_2$ (99.99%), $Co(CH_3COO)_2$ (99.99%), $Co(CH_3COO)_2{\cdot}4H_2O$ (99.99%), $CuCH_3COO$ (97%), $Cu(CH_3COO)_2$ (98%), $Zn(CH_3COO)_2$ (99.99%), $Zn(CH_3COO)_2{\cdot}2H_2O$ (≥98%), $AgCH_3COO$ (99%) and anhydrous tetrahydrofuran (THF, ≥ 99.99%) were obtained from Sigma-Aldrich, Germany. Poly(vinyl)silazane Durazane 1800 was purchased from durXtreme Gmbh, Germany.

2.2. Synthesis of metal-containing precursors

All synthesis reactions were carried out under standard Schlenk technique in vacuum/argon-line. Schlenk flask was dried at 80 °C overnight before pumping under vacuum and filling with argon (>99.999%) for the synthesis. The chemical reactants were stored in an argon-filled glovebox (MBraun MB200B; O_2 and H_2O concentrations kept at < 0.1 ppm) to avoid the oxidation of the polymer or the metal acetates. 18 g of Durazane 1800 was first dissolved in 50 mL anhydrous tetrahydrofuran (THF) and then transferred into a dropping funnel. In another round-bottom flask, 1.44 g (which corresponds to 8 wt% relative to the weight of Durazane 1800) or 7.2 g (which corresponds to 40.0 wt% relative to the weight of Durazane 1800) of metal acetate was dispersed in 50 mL anhydrous THF. The reaction vessel was then immediately removed from the glovebox after connecting round-bottom flask with the dropping funnel and the round-bottom flask was submerged in the ice bath (−6 °C). Before mixing the two solutions together, the round-bottom flask was connected with Schlenk vacuum/argon-lines. The synthesis process was continued under argon flow and stirring for 24 h at room temperature until the end of gas liberation. Finally, the THF solvent was removed under vacuum for at least 5 h and the synthesized metal-containing precursors were collected in the glovebox.

2.3. Pyrolysis of the synthesized metal-containing precursors

Pyrolysis of the synthesized metal-containing precursors was performed in a tube furnace with Schlenk tube under flowing argon (approximately 40 mL/min) applying two different pyrolyzed temperature of 700 °C and 1100 °C. The precursors were heated from room temperature to 250 °C with a rate of 50 °C h^{-1}, hold for 2 h at 250 °C, from 250 °C to 700 °C or 1100 °C with a rate of 50 °C h^{-1}, hold for 3 h at 700 °C or 1100 °C, finally cooled to room temperature with a rate of 180 °C h^{-1}.

2.4. Characterizations

Fourier Transform Infrared Spectroscopy (FTIR) in attenuated total reflectance (ATR) mode was carried out in Thermo Fisher Scientific Nicolet iS5 (USA) in the range of 4000 cm^{-1} to 550 cm^{-1}. X-ray photoelectron spectroscopy (XPS) was performed with K-Alpha TM (Thermo Scientific, USA). X-ray absorption near-edge spectroscopy (XANES) was collected in the transmission mode at beamline KMC-2 of the BESSY-II synchrotron light source at Berlin, Germany, equipped with a graded Si–Ge (111) double crystal monochromator [39]. The samples were prepared in the form of powder applied onto adhesive Kapton tape. High harmonics were rejected by detuning the monochromator so that the intensity of the beam on the samples was 65 % of the maximum possible intensity. Reference spectra were simultaneously measured for energy calibration. XANES data were analyzed with the Athena software package. The polymer to ceramic conversion was investigated in argon with a heating rate of 5 °C min^{-1} with thermal gravimetry analysis (TGA) on STA 409 PC LUXX (Netzsch, Germany) coupled with a mass spectrometer OMNi Star GSD 320 (Pfeiffer Vacuum, Germany). The X-ray diffraction was performed with Bruker AXS D8 ADVANCE X-ray diffractometer with CoKα1. Measurements were carried out between 10 and 90° 2θ value, with a step size of 0.02° and 3 s per step. The Inductively coupled plasma-optical emission spectrometry (ICP-OES) analysis was used to confirm the amount of Si and metal in the ceramic nanocomposites pyrolyzed at 1100 °C under argon.

3. Results and discussion

3.1. Chemical structures of synthesized precursors

Fig. 1 and Fig. S3 show the chemical structure of the poly(vinyl) silazane (Durazane 1800), which is a copolymer containing 20% of methyl/vinyl and 80% of methyl/hydride substituted silazane units, and different metal acetates used in the synthesis of metal-containing polysilazane precursors. It can be clearly seen that the reaction of some metal acetates such as $Mn(Ac)_3.2H_2O$, $Fe(Ac)_2$, $Co(Ac)_2$, $Co(Ac)_2.4H_2O$, CuAc, $Cu(Ac)_2$ with Durazane 1800 is accompanied with a change in the colour of these metal acetates into black, while the reaction of AgAc with Durazane 1800 lead to the formation of grey precipitates. In contrast, no change in colour was observed during the reaction of $Zn(Ac)_2$, $Zn(Ac)_2.2H_2O$, and $Mn(Ac)_2$ with the polymer. However, gaseous bubbles were observed during the reactions of all these metal acetates with the polymer regardless of whether colour changes or not, suggesting the releasing of some gases such as H_2 or NH_3 (see Fig. S3). It seems there is no reaction happened between $Mg(Ac)_2.4H_2O$, $Mn(Ac)_2$ and Durazane 1800 at this temperature (−6 °C), because no colour changes and gaseous bubbles can be observed during reaction. The status of the synthesized metal-containing precursors is summarized in Table 1.

Fig. 2 shows the ATR-FTIR spectra of Durazane 1800 polymer as well as the synthesized metal-containing precursors using 40 wt% of different metal acetates relative to the weight of Durazane 1800. The spectrum of Durazane 1800 shows the expected absorption bands of polysilazane, as

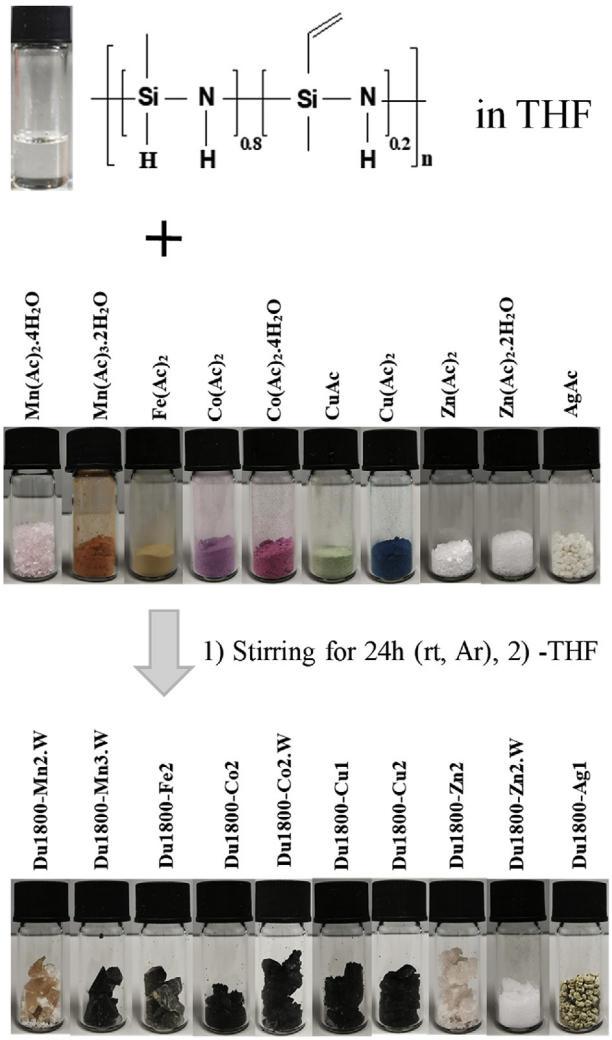

Fig. 1. Schematic of the synthesis of metal-containing precursors Du1800-Mn2.W, Du1800-Mn3.W, Du1800-Fe2, Du1800-Co2, Du1800-Co2.W, Du1800-Cu1, Du1800-Cu2, Du1800-Zn2, Du1800-Zn2.W and Du1800-Ag1 from Durazane 1800 and metal acetates $Mn(Ac)_2.4H_2O$, $Mn(Ac)_3.2H_2O$, $Fe(Ac)_2$, $Co(Ac)_2$, $Co(Ac)_2.4H_2O$, CuAc, $Cu(Ac)_2$, $Zn(Ac)_2$, $Zn(Ac)_2.2H_2O$ and AgAc.

reported in the literature [38,40]. The absorption bands at 3382 cm^{-1} and 1162 cm^{-1} can be assigned to the N–H stretching and the vibration of -NH- unit bridging two silicon atoms, respectively. The band at 1590 cm^{-1} represents the C═C stretching vibration, along with the vinyl group absorbs at 1402 cm^{-1} due to the scissoring of terminal methylene. The C–H vibration of vinyl group occurs at 3042 cm^{-1}. The strong absorption band assigned to Si–H vibration appears at 2116 cm^{-1}. The characteristics band of Si–CH_3 groups locates at 1255 cm^{-1}, coupled with C–H stretching at 2953 cm^{-1} and 2896 cm^{-1}. A decrease in the intensity of absorption bands at 2116 cm^{-1} and 1162 cm^{-1}, which are attributed to the Si–H and Si–NH–Si groups, respectively, are observed in the spectra of all the metal-containing polymer precursors. Moreover, for precursors Du1800-Mn3.W, Du1800-Fe2, Du1800-Co2, Du1800-Co2.W, Du1800-Cu1, Du1800-Cu2, the band at 3042 cm^{-1}, which is assigned to the vibration of C–H bond in the vinyl groups, is vanished. This result suggests that hydrosilylation reaction between Si–H and -Si-CH═CH_2 may take place at room temperature, leading to the formation of carbosilane bonds (-Si-C-C-Si-) (see Scheme 2 in Fig. S3a). It has been reported that hydrosilylation reaction usually starts at 100–120 °C in pure polysilazanes [41,42]. However, the presence of inorganic catalysts such as transition metals or metal complexes could remarkably increase the hydrosilylation rate as well as lower the temperature required for hydrosilylation [43–46]. Simultaneously, the absorption bands observed at 1712 and 1369 cm^{-1}, which can be assigned to C═O and -COO^{-1}, respectively, in the spectra of all the synthesized metal-containing precursors [47], indicating the reaction between the polymer and acetate groups (see Scheme 1 in Fig. S3a and Fig. S3b). However, the broad absorption band located at around 1561 cm^{-1} and 1414 cm^{-1} can be attributed to the -COO^{-1} group that from the unreacted metal acetates [47]. The ATR-FTIR spectra of some metal acetates are shown in Fig. S2. These results point out at three main effects took place during the reaction of Durazane 1800 polymer with metal acetates: (i) the reaction between the acetate groups of metal acetate with the silicon centers of Durazane 1800, causing the decrease in the number of Si–H and Si–NH–Si groups in the obtained precursors and the concomitant evolution of gaseous H_2 and NH_3 during the synthesis (Fig. S3a, Scheme 1 and Fig. S3b), (ii) the hydrosilylation reaction between -Si-H and -Si-CH═CH_2 groups in the Durazane 1800 with the formation of carbosilane bonds, leading to the formation of carbosilane bonds –Si-C-C-Si- (Fig. S3a, Scheme 2), and (iii) hydrolysis reactions of different functional groups, such as Si–H and Si–N–H, yielding silanol groups that are further condensed to form highly crosslinked Si–O–Si bonds (Fig. S3a, Scheme 3–5).

Fig. S1 shows the ATR-FTIR spectra of metal-containing (Mn, Fe and Zn) polymer precursors prepared from corresponding metal acetate with different contents (i.e. 8 and 40 wt% that relative to the weight of Durazane 1800). The intensities of absorption bands at 2116, 1162 and 3042 cm^{-1}, which are attributed to the Si–H, Si–NH–Si and C–H groups, respectively, decreased remarkably with an increasing amount of metal acetate. Moreover, the intensity of absorption bands observed at 1712 and 1369 cm^{-1}, assigned to C═O and -COO^{-1}, respectively, increased with an increasing amount of metal acetate. These results suggest the increase in the hydrosilylation rate (see Scheme 2 in Fig. S3a) as well as the reaction between the polymer and acetate groups (see Scheme 1 in Fig. S3a and Fig. S3b) with an increasing amount of metal acetate. Moreover, the high amount of metal acetate is beneficial for an increasing ceramic yield after pyrolysis. Therefore, other metal-containing precursors were synthesized with 40.0 wt% of metal acetates relative to the weight of Durazane 1800.

3.2. *Oxidation states of metals in the synthesized precursors*

The oxidation states of incorporated transition metals in the synthesized metal-containing precursors are investigated by X-ray photoelectron spectroscopy. As shown in Fig. 3, XPS Mn 2p spectrum of Du1800-Mn2.W precursor can be fitted with doublet peak at 641.5 and 653.0 eV and satellites at 645.5 and 657.0 eV, which is in good agreement with the previous reports for MnO [48,49]. XPS Fe 2p spectrum of Du1800-Fe2 precursor can be deconvoluted into three doublet peaks. The doublet peak located at 707.0 and 719.9 eV can be assigned to the metallic iron Fe^0, while, the two additional doublets corresponding to oxidized iron Fe^{2+} and Fe^{3+} were observed at higher binding energies. The broad peaks at 715.4 and 729.0 eV are satellite peaks corresponding to Fe $2p_{3/2}$ and $2p_{1/2}$, respectively [50,51]. This result suggests the presence of unreacted $Fe(Ac)_2$ in the Du1800-Fe2 precursors, which agrees with XRD results (Fig. 6b). XPS Co 2p spectrum of Du1800-Co2 precursor can be fitted with doublet peak located at 780.9 and 797.0 eV and satellites at 785.3 and 802.4 eV, which is in good agreement with the previous reports for CoO [52,53]. In contrast, the XPS Cu 2p spectrum of Du1800-Cu2 precursor composed of only doublet peak at 932.4 and 952.5 eV, which is characteristic of metallic copper [54]. Similarly, only doublet peak is observed at 368.3 and 374.3 eV in the XPS Ag 3d spectrum of Du1800-Ag1 precursor, which is characteristic of metallic silver [55]. The XPS Zn 2p spectrum of Du1800-Zn2.W precursor exhibits the binding energies of Zn $2p_{3/2}$ at about 1021.7 eV and Zn $2p_{1/2}$ centred at 1044.8 eV. However, it is difficult to distinguish the oxidation state of Zn from this result because of the small difference between binding energies of Zn^0 and Zn^{2+} (i.e. ~0.3 eV). Therefore, we applied X-ray absorption

Table 1
Oxidation states of metal and phase composition of specimens obtained in the reaction between Durazane 1800 and metal acetates content of 40 wt % relative to the weight of Durazane 1800.

Metal acetates	The observations of the reaction	Synthesized precursors	Surface oxidation states of metal states in the synthesized precursors (XPS results)	Oxidation states of metals in the synthesized precursors (XANES results)	Phase compositions (XRD results)		
					Synthesized precursors	Nanocomposites pyrolyzed at 700 °C/ 3h Ar	Nanocomposites pyrolyzed at 1100 °C/ 3h Ar
$Mn(AC)_2.4H_2O$	Becomes dark pink, gaseous bubbles	Du1800-Mn2.W	Mn^{2+}		$Mn(Ac)_2.4H_2O$	amorphous	SiC, Si_2N_2O, Mn_5Si_3
$Mn(AC)_3.2H_2O$	Becomes black, gaseous bubbles	Du1800-Mn3.W			amorphous	amorphous	SiC, Si_2N_2O, Mn_5Si_3
$Fe(AC)_2$	Becomes black, gaseous bubbles	Du1800-Fe2	Fe^0, Fe^{2+}, Fe^{3+}		$Fe(Ac)_2$	Fe	SiC, Fe_5Si_3, C
$Co(AC)_2$	Becomes black, gaseous bubbles	Du1800-Co2	Co^{2+}		$Co(Ac)_2$	Co, Co_2Si	Co, Co_2Si, CoSi
$Co(AC)_2.4H_2O$	Becomes black, gaseous bubbles	Du1800-Co2.W			Co	Co, CoSi	CoSi
CuAC	Becomes black, gaseous bubbles	Du1800-Cu1			Cu, Cu_2O	Cu	Cu, Cu_3Si, Cu_4Si
$Cu(AC)_2$	Becomes black, gaseous bubbles	Du1800-Cu2	Cu^0	Cu^0	Cu, Cu_2O	Cu	Cu
$Zn(AC)_2$	No colour change, gaseous bubbles	Du1800-Zn2		Zn^{2+}	amorphous	Zn	Zn
$Zn(AC)_2.2H_2O$	No colour change, gaseous bubbles	Du1800-Zn2.W		Zn^{2+}	$Zn(AC)_2.2H_2O$	amorphous	amorphous
AgAc	Precipitates, gaseous bubbles	Du1800-Ag1	Ag^0		Ag	Ag	Ag

near-edge spectroscopy (XANES) to determine the oxidation state of Zn in this precursor.

Fig. 4a and c display the Cu K-edge of Du1800-Cu2 precursor and Zn K-edge XANES spectra of Du1800-Zn2, Du1800-Zn2.W precursors, as well as those Cu and Zn compounds used as reference materials. The latter contains Cu and Zn cations in defined oxidation states. The first derivatives of XANES spectra of these materials are shown in Fig. 4b and d. The XANES spectra of these specimens consist of two characteristic features. The pre-edge feature, which is observed in the K-edge XANES of most 3*d* elements, is attributed to the transitions from 1*s* orbital into the final bound state in 3*d* orbitals, while, the main absorption edge feature is due to the transitions from 1*s* orbital to *p*-orbitals. The energies of these two edge features depend on the oxidation state of 3*d* elements in the solid-state materials [56,57]. As shown in Fig. 4a, the main characteristic feature of Cu(II) XANES spectra is a shoulder at around 8988.0 eV, which can be attributed to 1s→4p transitions. A weak absorption peak at about 8977.0 eV can be clearly observed in the first derivative spectra of Cu(II) XANES (Fig. 4b). This peak is due to the dipole-forbidden, quadrupole-allowed 1s→3d electronic transition that indicates a significant feature for Cu(II) because there is no 3d vacancy in the Cu foil. As shown in the first derivative spectra of XANES, Du1800-Cu2 precursor exhibits the same peak position at 8981.0 eV with Cu foil and the small peak 8979.0 eV that located between Cu(II) and Cu foil. The Cu foil and Du1800-Cu2 precursor show the similar first derivative spectra. This is a strong indication of the predominant character of metallic Cu in Du1800-Cu2 precursor. The Zn K-edge normalized XANES spectra of Du1800-Zn2 and Du1800-Zn2.W precursors and their first derivative spectra of the XANES are shown in Fig. 4c and d, respectively. The d shell in Zn is fully occupied and so it is not possible to observe a pre-edge peak that is related to the 1s→3d electronic transition in the normalized

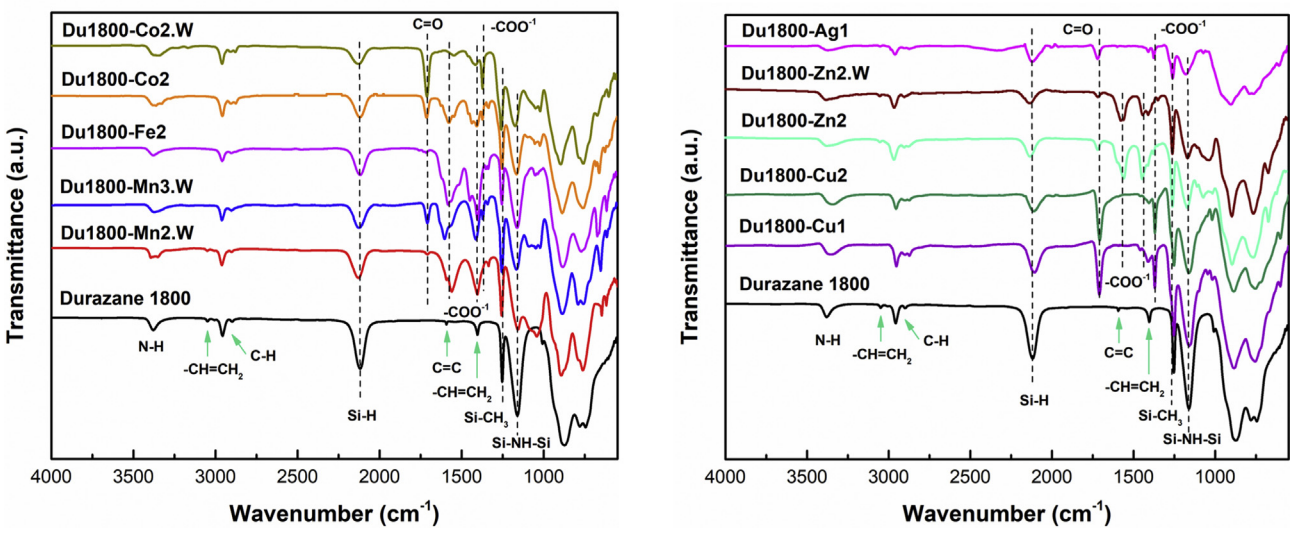

Fig. 2. The ATR-FTIR spectra of metal-containing polysilazane precursors derived from Durazane 1800 and metal acetates (all of them – at 40 wt% relative to the weight of Durazane 1800).

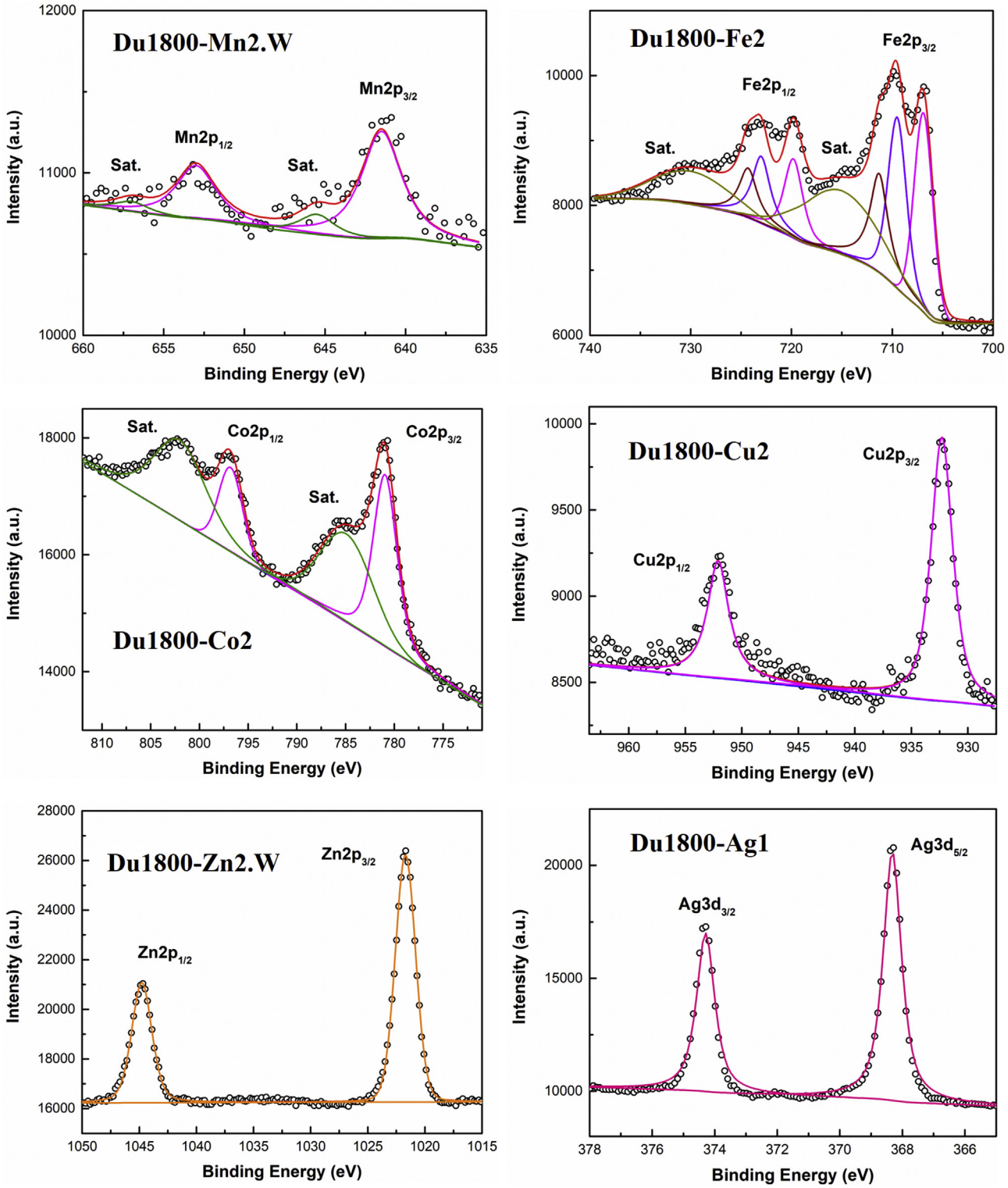

Fig. 3. X-ray photoelectron spectra (XPS) of Du1800-Mn2.W, Du1800-Fe2, Du1800-Co2, Du1800-Cu2, Du1800-Zn2.W, Du1800-Ag1 derived from Durazane 1800 and metal acetate content of 40 wt% relative to the weight of Durazane 1800.

XANES spectra as Cu. The peak at around 9661.6 eV, a prominent feature of Du1800-Zn2 and Du1800-Zn2.W precursors in their first derivative spectra, is between the peak position of ZnO and zinc acetate but very close to that of ZnO (9661.3 eV), suggesting the formation of Zn^{2+}-compounds (e.g. ZnO) in Du1800-Zn2 and Du1800-Zn2.W precursors. These results are in good agreement with XPS results. The oxidation states of incorporated transition metals in the synthesized metal-containing precursors as revealed from XPS and XANES characterizations are listed in Table 1.

The completeness of the reaction between the Durazane 1800 polymer and different metal acetates could be proven from the final oxidation states of different transition elements in the synthesized metal-containing polysilazane precursors. As shown in Table 1, which summarized the results of XPS, XANES and XRD characterization, no metal acetates

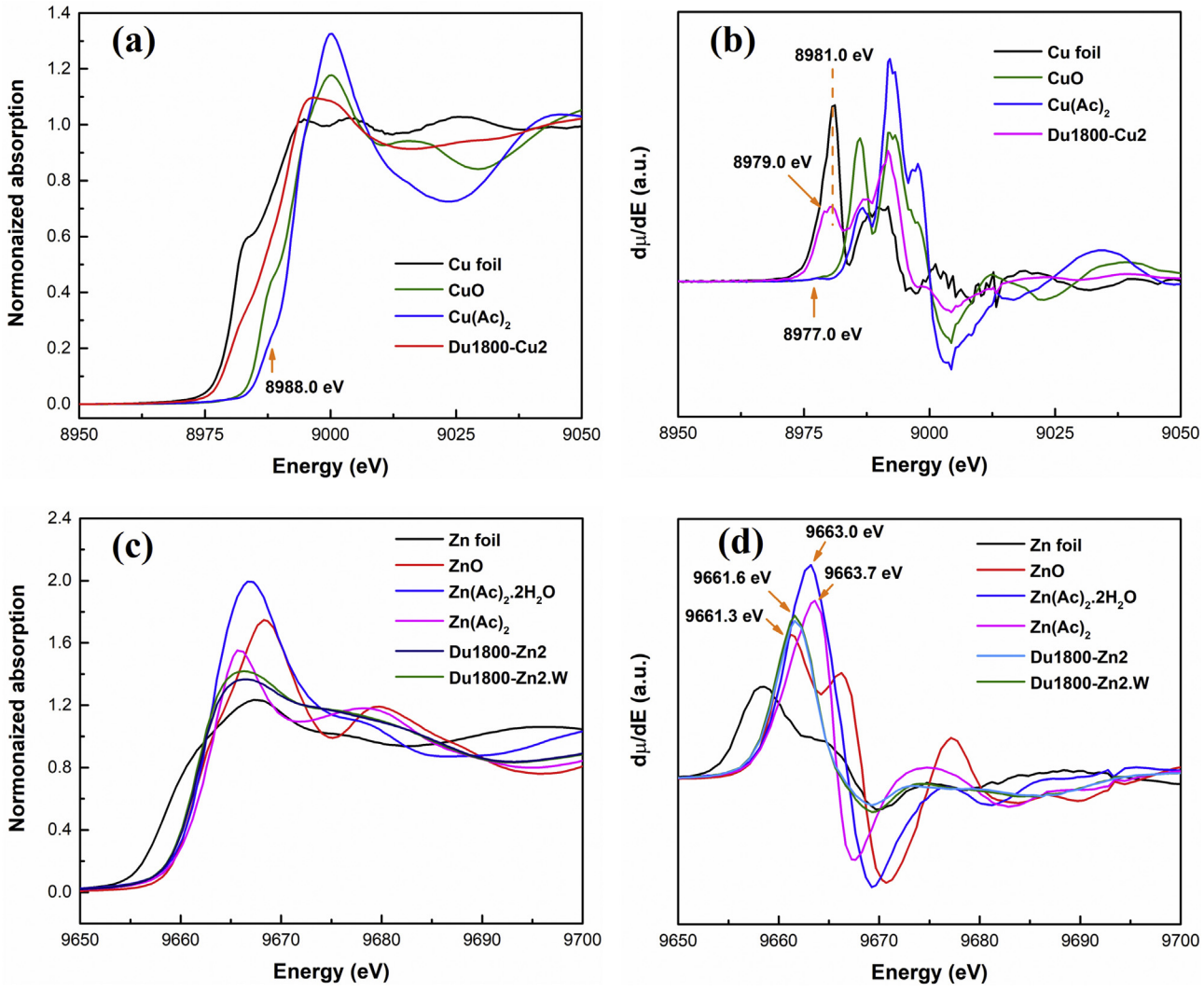

Fig. 4. The normalized X-ray absorption near-edge spectra (XANES) at (a) Cu K-edge of Du1800-Cu2 precursor compared as well as the reference materials (Cu foil, CuO and $Cu(Ac)_2$) (c) Zn K-edge of Du1800-Zn2 and Du1800-Zn2.W precursors compared to the reference materials (Zn foil, ZnO, $Zn(Ac)_2$ and $Zn(Ac)_2.2H_2O$). Their first derivative spectra are shown in (b), (d), respectively.

residue were observed in the precursor samples when transition elements present in the metal states, suggesting the completeness of the chemical reaction between the Durazane 1800 polymer and corresponding metal acetates. In contrast, the transition elements exist as divalent cations in the synthesized precursors due to the incomplete of the reaction and the presence of some metal acetate residues in the samples.

3.3. Cross-linked precursors and their conversion into metal/SiOCN ceramic nanocomposites

In the next step, the cross-linking process of the synthesized metal-containing precursors and their conversion into metal/SiOCN ceramic nanocomposites under argon atmosphere were investigated by a Simultaneous Thermal Analysis (STA) characterization (Fig. 5 and Fig. S2). As shown in Fig. 5, the differential thermal analysis (DTA) of Durazane 1800 in argon atmosphere shows two exothermic peaks at 250 °C and 550 °C accompanied by a weight loss of 25% and 9%, respectively. In-situ MS spectra collected during the pyrolysis process reveals that the weight loss at 250 °C can be attributed to the transamination reaction by detecting the evolution of NH_3 gases ($m/z = 17$) and CH_4 ($m/z = 16$) evolution originates from the decomposition of Si–CH_3 or the cleavage of C–C bonds. The dehydrocoupling reactions between Si–H/Si–H and Si–H/N–H groups, which can be identified by the evolution of hydrogen ($m/z = 2$), could be responsible for the second stage of weight loss at 550 °C. No mass loss or gas evolutions are observed above 900 °C, suggesting the complete transformation of Durazane 1800 polymer into the amorphous SiCN ceramics. The ceramic yield resulted from polysilazane Durazane 1800 after completing pyrolysis at 1100 °C is 66%. These results agree with other previous reports for polysilazanes [58]. On the other hand, the pyrolysis of the synthesized metal-containing precursors shows different results in comparison with those of pure polymer. For instance, the in-situ MS spectra of all metal-containing precursors exhibit the evolution of CO_2 ($m/z = 44$) below 400 °C, which is not observed for the pure polymer and might be due to the thermal decomposition of acetate group from metal acetates. Moreover, most of metal-containing precursors show a continuous weight loss during the whole pyrolysis step up to 1100 °C with the evolution of H_2. The weight loss observed at low temperature (i.e. < 200 °C) from some metal-containing precursors such as Du1800-Co2, Du1800-Co2.W, Du1800-Cu1, Du1800-Cu2 and Du1800-Zn2 is accompanied with the evolution of NH_3 ($m/z = 17$) gas, suggesting the adsorption of some ammonia residues on the surface of metal-containing precursors. This ammonia residue could be formed during the reaction of metal acetates and Durazane 1800 [34]. As shown in Table 2, most of the synthesized metal-containing precursors exhibited higher ceramic yields if compared with pure polymer, which can be explained by the increase in the cross-linking degree of the precursors

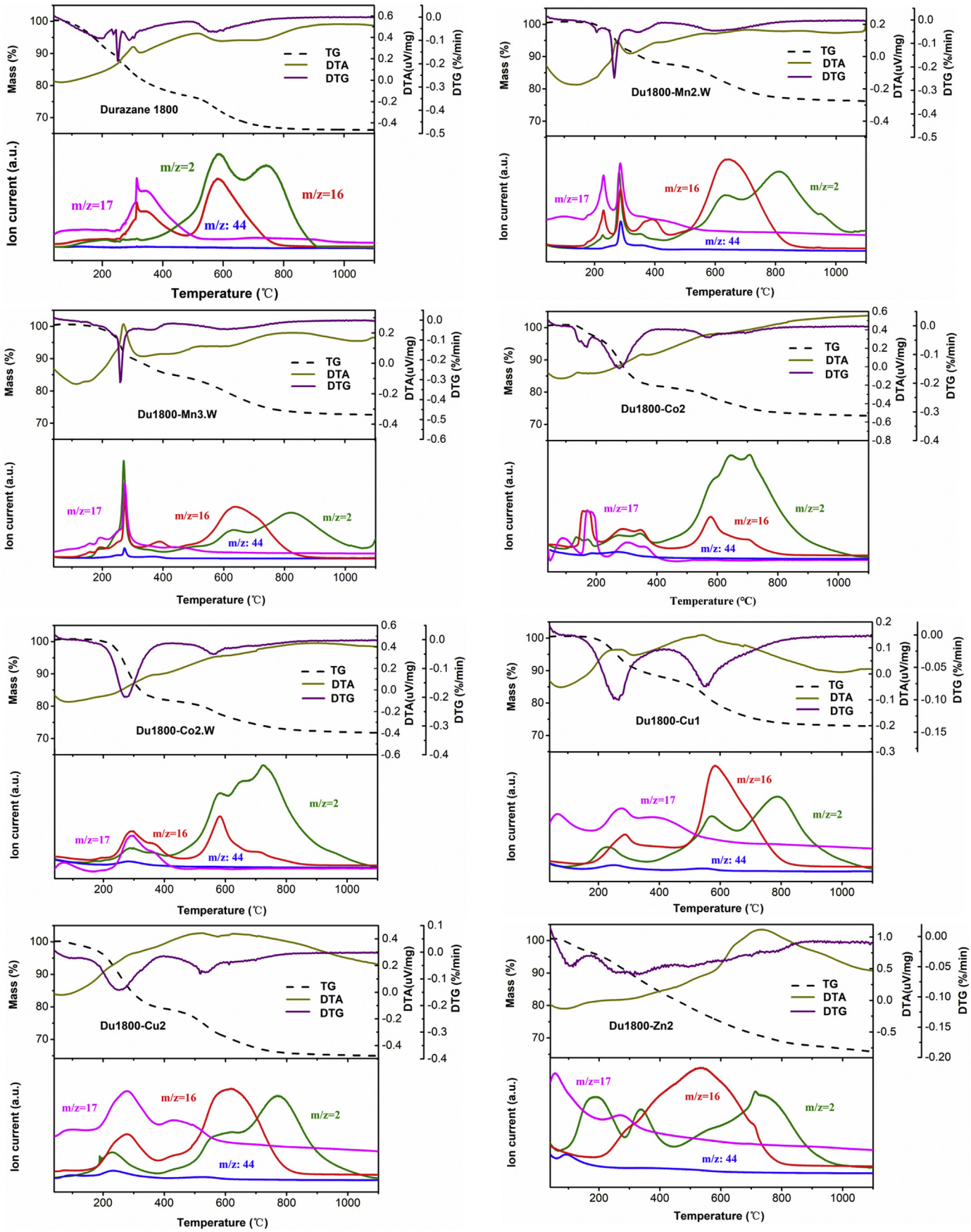

Fig. 5. Results of simultaneous thermal analysis (upper panels)-mass spectrometry (bottom panels) of Durazane 1800, Du1800-Mn2.W, Du1800-Mn3.W, Du1800-Co2, Du1800-Co2.W, Du1800-Cu1, Du1800-Cu2 and Du1800-Zn2 samples.

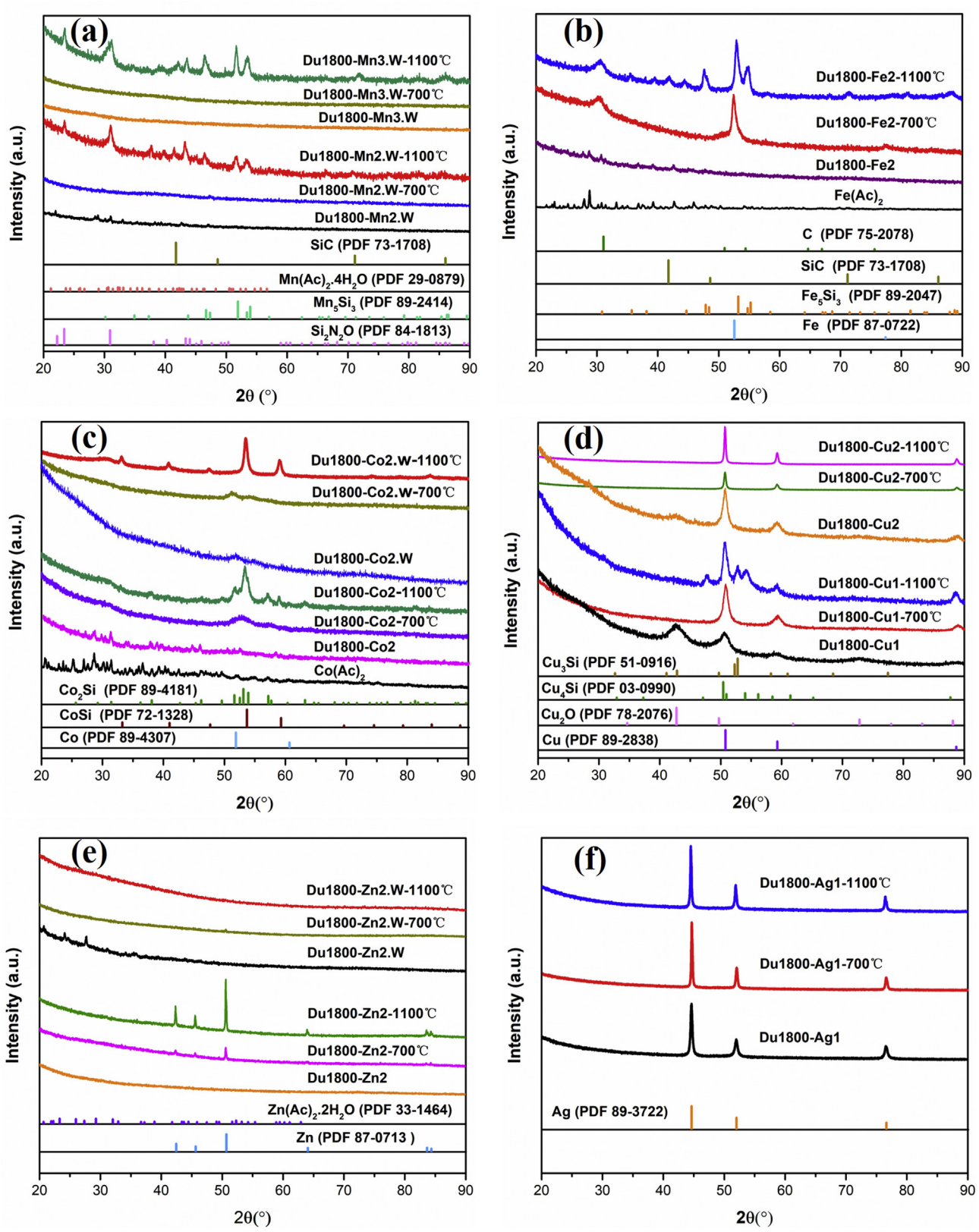

Fig. 6. XRD patterns of synthesized metal-containing precursors from Durazane 1800 and metal acetates content of 40 wt % relative to the weight of Durazane 1800 as well as their derived ceramic nanocomposites pyrolyzed at 700 °C and 1100 °C under argon for 3h.

Table 2
Ceramic yields and element (Si, metal) composition (ICP-OEM results) of the metal-containing nanocomposites pyrolyzed at 1100 °C for 3h under argon.

Polymer precursor	Expected ceramic yields (%)	Ceramic yields (%)	Expected Si:M (Weight ratio)	Si content (wt%)	Metal content (wt%)	Si:M (Weight ratio)
Durazane 1800	–	66		45.05	–	–
Du1800-Mn2.W	53.57	76.3	3.36	31.86	9.13	3.49
Du1800-Mn3.W	53	72.6	3.68	35.23	7.55	4.67
Du1800-Fe2	56.3	72.8	2.35	35.43	10.37	3.42
Du1800-Co2	56.7	72.8	2.27	35.58	9.6	3.7
Du1800-Co2.W	53.9	71.7	3.19	32.53	9.81	3.32
Du1800-Cu1	62	72.8	1.46	36	13.03	2.76
Du1800-Cu2	57.1	64.9	2.16	30.86	12.53	2.46
Du1800-Zn2	57.3	65.7	2.12	36.45	13.36	2.73
Du1800-Zn2.W	55.7	66.3	2.53	42.82	9.42	4.55
Du1800-Ag1	65.6	77.7	1.17	26.83	28.97	0.93

upon chemical modification with metal acetates. However, Du1800-Cu2 and Du1800-Zn2 precursors show a ceramic yield of 64.9% and 65.7%, respectively, which are slightly lower than that of Durazane 1800. In general, the ceramic yields obtained from STA measurement were found to be higher than the expected ceramic yields (calculated from the weight loss of individual polysilazane and metal acetate used without chemical reaction between them), which can be explained by the increase in the degree of cross-linking of the polymer due to the presence of metal acetates.

Furthermore, the metal content in ceramics obtained by pyrolysis of synthesized metal-containing precursors at 1100 °C under argon environment was also confirmed by ICP characterizations. As shown in Table 2, all the metals were successfully introduced inside the ceramic matrix. The weight ratio of Si:M in most pyrolyzed samples were found in good agreement with the experimental weight ratio used in the synthesis of the metal-containing precursors.

3.4. The composition of pyrolyzed precursors

In the next step, the crystallinity and phase compositions of the metal-containing precursors as well as their ceramic products obtained from pyrolysis in argon atmosphere at 700 °C and 1100 °C have been determined by XRD characterization and shown in Fig. 6 and Fig. S5-S8. As shown in Fig. 6a and Fig. S5, XRD pattern of Mn-containing Precursor Du1800-Mn2.W obtained from the reaction of Durazane 1800 with $Mn(Ac)_2.4H_2O$ exhibits some XRD reflections, which can be indexed to the monoclinic structure (SG: P21/c) of $Mn(Ac)_2.4H_2O$. In contrast, no XRD reflections are observed in the XRD pattern of Mn-containing precursor Du1800-Mn3.W obtained from the reaction of Durazane 1800 with $Mn(Ac)_3.2H_2O$, indicating the amorphous structure of the precursor. This result suggests $Mn(Ac)_3.2H_2O$ is fully reacted with the polymer, while, $Mn(Ac)_2.4H_2O$ is partially reacted at these reaction conditions. However, the pyrolysis of both Du1800-Mn2.W and Du1800-Mn3.W precursors at 700 °C results in the formation of amorphous ceramic products, while, crystalline Mn_5Si_3 (PDF No. 89–2414), Si_2N_2O (PDF No. 84–1813) and β-SiC (PDF No. 73–1708) phases are formed in both samples with increasing the pyrolysis temperature to 1100 °C. As reported in Ref. [12,59], MnO can be reduced by methane gas at 760 °C and can undergo carbothermal reduction in the presence of hydrogen at 920 °C, forming manganese carbide. Therefore, the formation of Mn_5Si_3 in nanocomposites derived from Mn-containing precursors Du1800-Mn2.W and Du1800-Mn3.W that pyrolyzed at 1100 °C under argon could be resulted from the reaction of the formed manganese carbide with the SiOCN matrix, which agrees with previous work [12]. In pure SiOCN ceramic, crystalline Si_2N_2O phase normally occurs at around 1500 °C [60], while in Mn/SiOCN nanocomposites, Si_2N_2O and SiC have been formed at much lower temperature. According to Ref. [61], when the N/O ratio in Si–O–C–N system is close to 2, nanoclusters of stoichiometric Si_2N_2O may be formed even with a positive enthalpy of formation. These interesting results suggest the introduction of manganese into SiOCN ceramic can greatly lower the crystalline temperature of Si_2N_2O and SiC from amorphous SiOCN ceramic.

Similar to $Mn(Ac)_2.4H_2O$, $Fe(Ac)_2$ is not fully reacted with the polymer as few of its corresponding XRD reflections are observed in the XRD pattern of Fe-containing precursor Du1800-Fe2 (Fig. 6b and Fig. S6). This result is good agreement with XPS results (Fig. 3) that suggests the presence of both Fe^0 and Fe^{2+} ions in the sample. The pyrolysis of this precursor at 700 °C leads to the formation of metallic iron phase (PDF No. 87–0722) and small amounts of graphitic carbon (PDF No. 75–2078), suggesting that the $Fe(Ac)_2$ residue and iron oxides in precursor Du1800-Fe2 are further reduced to form metallic Fe phase during the thermal cross-linkage process. According to Ref. [62], as iron oxides are thermodynamically unstable in this temperature range with respect to the carbothermal reduction to metallic Fe. Further increase in the pyrolysis temperature to 1100 °C results in the formation of Fe_5Si_3 (PDF No: 89–2047) and β-SiC (PDF No. 73–1708) phases due to the reaction of Fe metal with the amorphous SiOCN matrix. The formation β-SiC phase is consistent with previous studies reported that β-SiC nanofibers could be grown in polymer-derived ceramics via the well-known vapor–liquid–solid (VLS) mechanism with Fe acting as the metal catalyst [63,64]. As iron shows good catalytic properties for the formation of graphitic carbon in PDCs during pyrolysis process [35], we can easily find the graphitic carbon peak on the XRD pattern and carbon nanotubes in the microstructure. Therefore, we can suppose the formation of SiC can be attributed to the reaction of SiO(g) with graphitic carbon ($SiO(g) + 2C(s) \rightarrow SiC(s) + CO(g)$) or CO ($SiO(g) + 3CO(g) \rightarrow SiC(s) + 2CO_2(g)$) [63,64].

XRD results of Co-containing precursors Du1800-Co2 and Du1800-Co2.W (Fig. 6c and Fig. S7) reveal that the reaction of hydrous $Co(Ac)_2.4H_2O$ with Durazane 1800 polymer is completed, leading to the formation of Co metal in amorphous SiOCN matrix. In contrast, anhydrous $Co(Ac)_2$ is partially reacted with the polymer as XRD reflections corresponding to $Co(Ac)_2$ are observed in the XRD pattern of Du1800-Co2 precursor. The pyrolysis of Du1800-Co2 precursors at 700 °C leads to the formation of Co metal and Co_2Si. With further increasing pyrolysis temperature to 1100 °C results in the formation of CoSi phase in the sample. The formation of cobalt silicide in PDCs can be attributed to the reaction of cobalt metal with the SiOCN matrix. The high pyrolysis temperature will facilitate the reaction of Si in SiOCN matrix with residual Co metal to form metastable Co_2Si first and then CoSi. These results are consistent with previous works showed that the metastable Co_2Si phase is usually formed in PDCs at lower pyrolysis temperature before the formation of CoSi at higher temperature [6,26,63]. However, for Du1800-Co2.W precursors, silicon-rich cobalt silicide phase CoSi starts to be crystallized by pyrolysis at 700 °C due to the reaction of Co metal present in the precursor sample with Si in SiOCN matrix. With increasing the pyrolysis temperature to 1100 °C, the formation of CoSi phase is completed and no more Co metal observed in this sample. The difference in the phase composition between Du1800-Co2 and Du1800-Co2.W samples after pyrolysis can be explained by the difference in chemical properties of cobalt compound in the precursor samples as Co metal and $Co(Ac)_2$ are found in Du1800-Co2.W and Du1800-Co2

precursors, respectively. Similarly, the chemical structure of polymeric precursors in both samples can also be different that will affect silicon diffusion rate to react with Co metal to form cobalt silicide phases during pyrolysis.

On the other hand, XRD patterns of Du1800-Cu1 and Du1800-Cu2 precursors (Fig. 6d and Fig. S8) show that the reaction of anhydrous CuAC and $Cu(Ac)_2$ with Durazane 1800 polymer results in the formation of Cu and Cu_2O. Comparing the intensities of XRD reflections corresponding to Cu and Cu_2O phases in both samples indicates that Du1800-Cu1 sample has a higher amount of Cu_2O phase if compared with that in Du1800-Cu2 sample. These results suggest the low stability of CuAC under these synthesis conditions; thus, it is transformed into Cu_2O before reacting with the polymer. However, this Cu_2O phase is metastable and reduced to metallic Cu by pyrolyzing precursor at 700 °C. The formed Cu metal in Du1800-Cu2 precursor is found to be very stable under both pyrolysis temperatures. In contrast, the pyrolysis of Du1800-Cu1 precursors at 1100 °C leads to the formation of copper silicide phases (i.e. Cu_3Si and Cu_4Si) due to the reaction of Cu metal with the amorphous SiOCN matrix, which is in good agreement with reported Cu–Si phase diagram [65]. The formation of copper silicide phases at 1100 °C in Du1800-Cu1 but not in Du1800-Cu2 sample can be explained by the difference in the crystallite size of Cu metal in both samples. As it can be seen from Fig. 6d, the XRD reflections corresponding to Cu metal in Du1800-Cu1 pyrolyzed at 700 °C are much broader than those of Cu phase in Du1800-Cu2 sample pyrolyzed at the same temperature, suggesting the smaller size of Cu crystallites in Du1800-Cu1 if compared with that in Du1800-Cu2 sample. This small crystallite size of Cu metal might facilitate its reaction with Si in the SiOCN matrix to form copper silicide phases.

As shown in Fig. 6e, crystalline $Zn(AC)_2.2H_2O$ is observed in the XRD pattern of Du1800-Zn2.W precursor and no crystalline Zn-based compounds are indicated after the pyrolysis of this precursor at 700 °C and 1100 °C. In contrast, despite Du1800-Zn2 precursor also exhibits an amorphous structure but not crystalline zinc acetate phase can be found in this precursor. Moreover, the pyrolysis of Du1800-Zn2 precursor at 700 °C and 1100 °C results in the formation of Zn metal, which is consistent with previous reported Zn–Si phase diagram [66]. These results suggest that Durazane 1800 polymer has been reacted with anhydrous $Zn(AC)_2$ but not with hydrous $Zn(AC)_2.2H_2O$.

XRD pattern of Du1800-Ag1 (Fig. 6f) precursor shows the formation of Ag metal after the reaction of anhydrous AgAc with Durazane 1800 polymer. The stability of formed Ag metal even after the pyrolysis of Du1800-Ag1 precursor at 1100 °C is in good agreement with the reported phase diagram of Ag–Si that suggests no possible reactions between Si and Ag at these conditions [67]. The phase compositions of the synthesized precursors as well as pyrolyzed nanocomposites are summarized in Table 1.

4. Conclusions

In this report, we propose a one-step chemical route to synthesize metal-containing (Mn, Fe, Co, Cu, Zn and Ag) precursors through a very simple chemical reaction of metal acetates with poly(vinyl)silazane Durazane 1800 in an ice bath under argon atmosphere. The ATR-FTIR spectra reveal the decreased signal intensity that attributed to the Si–H (2116 cm^{-1}) and Si–NH–Si (1162 cm^{-1}) groups. In addition, for precursors Du1800-Mn3.W, Du1800-Fe2, Du1800-Co2, Du1800-Co2.W, Du1800-Cu1, Du1800-Cu2, the absorption band corresponding toC–H vibration at 3042 cm^{-1} that related to the vinyl groups are vanished. This means hydrosilylation reaction between -Si-H and -Si-CH═CH_2 may happen at room temperature. The XPS and XRD results of the synthesized precursors indicate the direct formation of metallic phase in precursors Du1800-Fe2, Du1800-Co2.W, Du1800-Cu1, Du1800-Cu2 and Du1800-Ag1 after the reaction. Metal or metal silicide containing nanocomposites can be obtained when the synthesized precursors are pyrolyzed at 700 °C and 1100 °C for 3h under argon atmosphere. However, the reaction mechanism between metal acetates and Durazane 1800 is still unclear, and further discussion will be conducted in our future work.

Acknowledgements

We would like to thank Dr. Julia Kohl and Prof. Matthias Drieß for the ATR-FTIR measurement, Harald Link for ICP-OES measurements, Heinz Sap for TG-MS measurement, as well Shuang Li for XPS measurements, all from Technische Universität Berlin. J. W. acknowledges financial support from China Scholarship Council (201604910900). We acknowledge support by the German Research Foundation and the Open Access Publication Fund of TU Berlin.

Appendix A. Supplementary data

Supplementary data to this article can be found online at https://doi.org/10.1016/j.oceram.2020.100001.

References

[1] D. Seyferth, H. Lang, C.A. Sobon, J. Borm, H.J. Tracy, N. Bryson, Chemical modification of preceramic polymers: their reactions with transition metal complexes and transition metal powders, J. Inorg. Organomet. Polym. 2 (1) (1992) 59–77.
[2] M. Birot, J.-P. Pillot, J. Dunogues, Comprehensive chemistry of polycarbosilanes, polysilazanes, and polycarbosilazanes as precursors of ceramics, Chem. Rev. 95 (5) (1995) 1443–1477.
[3] P. Colombo, G. Mera, R. Riedel, G.D. Soraru, Polymer-derived ceramics: 40 years of research and innovation in advanced ceramics, J. Am. Ceram. Soc. 93 (7) (2010) 1805–1837.
[4] P. Greil, Active-filler-controlled pyrolysis of preceramic polymers, J. Am. Ceram. Soc. 78 (4) (1995) 835–848.
[5] E. Ionescu, H.-J. Kleebe, R. Riedel, Silicon-containing polymer-derived ceramic nanocomposites (PDC-NCs): preparative approaches and properties, Chem. Soc. Rev. 41 (15) (2012) 5032–5052.
[6] M. Zaheer, T. Schmalz, G. Motz, R. Kempe, Polymer derived non-oxide ceramics modified with late transition metals, Chem. Soc. Rev. 41 (15) (2012) 5102–5116.
[7] M.S. Bazarjani, M.M. Müller, H.-J. Kleebe, C. Fasel, R. Riedel, A. Gurlo, In situ formation of tungsten oxycarbide, tungsten carbide and tungsten nitride nanoparticles in micro-and mesoporous polymer-derived ceramics, J. Mater. Chem. 2 (27) (2014) 10454–10464.
[8] M. Seifollahi Bazarjani, M.M. Müller, H.-J. Kleebe, Y. Jüttke, I. Voigt, M. Baghaie Yazdi, L. Alff, R. Riedel, A. Gurlo, High-temperature stability and saturation magnetization of superparamagnetic nickel nanoparticles in microporous polysilazane-derived ceramics and their gas permeation properties, ACS Appl. Mater. Interfaces 6 (15) (2014) 12270–12278.
[9] T. Erny, M. Seibold, O. Jarchow, P. Greil, Microstructure development of oxycarbide composites during active-filler-controlled polymer pyrolysis, J. Am. Ceram. Soc. 76 (1) (1993) 207–213.
[10] M. Seibold, P. Greil, Thermodynamics and microstructural development of ceramic composite formation by active filler-controlled pyrolysis (AFCOP), J. Eur. Ceram. Soc. 11 (2) (1993) 105–113.
[11] X. Yan, X.N. Cheng, C.S. Li, R. Hauser, R. Riedel, Synthesis and Low Temperature Magnetic Properties of Metal Elements Filled Polymer-Derived SiCN Ceramic Composites, Materials Science Forum, Trans Tech Publ, 2007, pp. 2269–2272.
[12] X. Yan, X.N. Cheng, G.C. Han, R. Hauser, R. Riedel, Synthesis and Magnetic Properties of Polymer Derived metal/SiCN Ceramic Composites, Key Engineering Materials, Trans Tech Publ, 2007, pp. 1485–1488.
[13] A. Saha, S.R. Shah, R. Raj, S.E. Russek, Polymer-derived SiCN composites with magnetic properties, J. Mater. Res. 18 (11) (2003) 2549–2551.
[14] M. Hojamberdiev, R.M. Prasad, K. Morita, M.A. Schiavon, R. Riedel, Polymer-derived mesoporous SiOC/ZnO nanocomposite for the purification of water contaminated with organic dyes, Microporous Mesoporous Mater. 151 (2012) 330–338.
[15] M. Hojamberdiev, R.M. Prasad, K. Morita, Y. Zhu, M.A. Schiavon, A. Gurlo, R. Riedel, Template-free synthesis of polymer-derived mesoporous SiOC/TiO_2 and SiOC/N-doped TiO_2 ceramic composites for application in the removal of organic dyes from contaminated water, Appl. Catal. B Environ. 115 (2012) 303–313.
[16] M. Seifollahi Bazarjani, M. Hojamberdiev, K. Morita, G. Zhu, G. Cherkashinin, C. Fasel, T. Herrmann, H. Breitzke, A. Gurlo, R. Riedel, Visible light photocatalysis with c-WO_{3-x}/WO_3×H_2O nanoheterostructures in situ formed in mesoporous polycarbosilane-siloxane polymer, J. Am. Chem. Soc. 135 (11) (2013) 4467–4475.
[17] K. Lu, D. Erb, M. Liu, Phase transformation, oxidation stability, and electrical conductivity of TiO_2-polysiloxane derived ceramics, J. Mater. Sci. 51 (22) (2016) 10166–10177.
[18] Y. Hou, L. Cheng, Y. Zhang, Y. Yang, C. Deng, Z. Yang, Q. Chen, P. Wang, L. Zheng, Electrospinning of Fe/SiC hybrid fibers for highly efficient microwave absorption, ACS Appl. Mater. Interfaces 9 (8) (2017) 7265–7271.

[19] Y. Wang, Y. Feng, X. Guo, Y. Liu, H. Gong, Electromagnetic and wave absorbing properties of Fe-doped polymer-derived SiCN ceramics, RSC Adv. 7 (73) (2017) 46215–46220.

[20] Y. Yu, L. An, Y. Chen, D. Yang, Synthesis of SiFeC magnetoceramics from reverse polycarbosilane-based microemulsions, J. Am. Ceram. Soc. 93 (10) (2010) 3324–3329.

[21] R.J. Corriu, N. Devylder, C. Guerin, B. Henner, A. Jean, Oligomers with silicon and transition metal groups: thermolysis of poly [1, 1′-bis (diorganosilylethynyl) ferrocenes] and poly [{(diorganosilylene) diacetylene} dicobalthexacarbonyls] to give iron silicide-and cobalt silicide-based ceramics, J. Organomet. Chem. 509 (2) (1996) 249–257.

[22] K. Kulbaba, A. Cheng, A. Bartole, S. Greenberg, R. Resendes, N. Coombs, A. Safa-Sefat, J.E. Greedan, H.D. Stöver, G.A. Ozin, Polyferrocenylsilane microspheres: synthesis, mechanism of formation, size and charge tunability, electrostatic self-assembly, and pyrolysis to spherical magnetic ceramic particles, J. Am. Chem. Soc. 124 (42) (2002) 12522–12534.

[23] A. Berenbaum, M. Ginzburg-Margau, N. Coombs, A.J. Lough, A. Safa-Sefat, J.E. Greedan, G.A. Ozin, I. Manners, Ceramics containing magnetic Co–Fe alloy nanoparticles from the pyrolysis of a highly metallized organometallic polymer precursor, Adv. Mater. 15 (1) (2003) 51–55.

[24] D.A. Rider, K. Liu, J.-C. Eloi, L. Vanderark, L. Yang, J.-Y. Wang, D. Grozea, Z.-H. Lu, T.P. Russell, I. Manners, Nanostructured magnetic thin films from organometallic block copolymers: pyrolysis of self-assembled polystyrene-block-poly (ferrocenylethylmethylsilane), ACS Nano 2 (2) (2008) 263–270.

[25] R. Petersen, D.A. Foucher, B.-Z. Tang, A. Lough, N.P. Raju, J.E. Greedan, I. Manners, Pyrolysis of poly (ferrocenylsilanes): synthesis and characterization of ferromagnetic transition-metal-containing ceramics and molecular depolymerization products, Chem. Mater. 7 (11) (1995) 2045–2053.

[26] S. Bourg, B. Boury, R.J. Corriu, Mixed Si/C/M/O ceramics from 2, 5-disilahexane/metal carbonyl (M [double bond, length as m-dash] Fe and Co), J. Mater. Chem. 8 (4) (1998) 1001–1006.

[27] R. Hauser, A. Francis, R. Theismann, R. Riedel, Processing and magnetic properties of metal-containing SiCN ceramic micro-and nano-composites, J. Mater. Sci. 43 (12) (2008) 4042–4049.

[28] X. Chen, Z. Su, L. Zhang, M. Tang, Y. Yu, L. Zhang, L. Chen, Iron nanoparticle-containing silicon carbide fibers prepared by pyrolysis of Fe (CO) 5-doped polycarbosilane fibers, J. Am. Ceram. Soc. 93 (1) (2010) 89–95.

[29] C. Luo, W. Duan, X. Yin, J. Kong, Microwave-absorbing polymer-derived ceramics from cobalt-coordinated poly (dimethylsilylene) diacetylenes, J. Phys. Chem. C 120 (33) (2016) 18721–18732.

[30] S. Yajima, T. Iwai, T. Yamamura, K. Okamura, Y. Hasegawa, Synthesis of a polytitanocarbosilane and its conversion into inorganic compounds, J. Mater. Sci. 16 (5) (1981) 1349–1355.

[31] F. Babonneau, G.D. Sorarù, Synthesis and characterization of Si; Zr; C; O ceramics from polymer precursors, J. Eur. Ceram. Soc. 8 (1) (1991) 29–34.

[32] E. Ionescu, C. Linck, C. Fasel, M. Müller, H.J. Kleebe, R. Riedel, Polymer-derived $SiOC/ZrO_2$ ceramic nanocomposites with excellent high-temperature stability, J. Am. Ceram. Soc. 93 (1) (2010) 241–250.

[33] E. Ionescu, B. Papendorf, H.J. Kleebe, F. Poli, K. Müller, R. Riedel, Polymer-derived silicon oxycarbide/hafnia ceramic nanocomposites. Part I: phase and microstructure evolution during the ceramization process, J. Am. Ceram. Soc. 93 (6) (2010) 1774–1782.

[34] M. Seifollahi Bazarjani, H.-J. Kleebe, M.M. Müller, C. Fasel, M. Baghaie Yazdi, A. Gurlo, R. Riedel, Nanoporous silicon oxycarbonitride ceramics derived from polysilazanes in situ modified with nickel nanoparticles, Chem. Mater. 23 (18) (2011) 4112–4123.

[35] T. Schmalz, T. Kraus, M. Günthner, C. Liebscher, U. Glatzel, R. Kempe, G. Motz, Catalytic formation of carbon phases in metal modified, porous polymer derived SiCN ceramics, Carbon 49 (9) (2011) 3065–3072.

[36] M. Zaheer, C.D. Keenan, J. Hermannsdörfer, E. Roessler, G.n. Motz, J.r. Senker, R. Kempe, Robust microporous monoliths with integrated catalytically active metal sites investigated by hyperpolarized 129Xe NMR, Chem. Mater. 24 (20) (2012) 3952–3963.

[37] S.M. Sachau, M. Zaheer, A. Lale, M. Friedrich, C.E. Denner, U.B. Demirci, S. Bernard, G. Motz, R. Kempe, Micro-/Mesoporous platinum–SiCN nanocomposite catalysts (Pt@ SiCN): from design to catalytic applications, Chem. A Eur. J. 22 (43) (2016) 15508–15512.

[38] M. Zaheer, G. Motz, R. Kempe, The generation of palladium silicide nanoalloy particles in a SiCN matrix and their catalytic applications, J. Mater. Chem. 21 (46) (2011) 18825–18831.

[39] D.M. Többens, S. Zander, KMC-2: an X-ray beamline with dedicated diffraction and XAS endstations at BESSY II, J. Large-scale Res. Facilities JLSRF 2 (2016) 49.

[40] P.J. Launer, Infrared analysis of organosilicon compounds: spectra-structure correlations, in: Silicone Compounds Register and Review 100, 1987.

[41] Y.D. Blum, D.B. MacQueen, H.-J. Kleebe, Synthesis and characterization of carbon-enriched silicon oxycarbides, J. Eur. Ceram. Soc. 25 (2–3) (2005) 143–149.

[42] G.D. Soraru, F. Dalcanale, R. Campostrini, A. Gaston, Y. Blum, S. Carturan, P.R. Aravind, Novel polysiloxane and polycarbosilane aerogels via hydrosilylation of preceramic polymers, J. Mater. Chem. 22 (16) (2012) 7676–7680.

[43] V.C. Gibson, S.K. Spitzmesser, Advances in non-metallocene olefin polymerization catalysis, Chem. Rev. 103 (1) (2003) 283–316.

[44] R. Jazzar, J. Hitce, A. Renaudat, J. Sofack-Kreutzer, O. Baudoin, Functionalization of organic molecules by transition-metal-catalyzed C (sp3); H activation, Chem. A Eur. J. 16 (9) (2010) 2654–2672.

[45] O. Daugulis, H.-Q. Do, D. Shabashov, Palladium-and copper-catalyzed arylation of carbon− hydrogen bonds, Acc. Chem. Res. 42 (8) (2009) 1074–1086.

[46] R. Giri, N. Maugel, J.-J. Li, D.-H. Wang, S.P. Breazzano, L.B. Saunders, J.-Q. Yu, Palladium-catalyzed methylation and arylation of sp2 and sp3 C− H bonds in simple carboxylic acids, J. Am. Chem. Soc. 129 (12) (2007) 3510–3511.

[47] D. Edwards, R. Hayward, Transition metal acetates, Can. J. Chem. 46 (22) (1968) 3443–3446.

[48] O. Bulavchenko, Z. Vinokurov, T. Afonasenko, P. Tsyrul'nikov, S. Tsybulya, A. Saraev, V. Kaichev, Reduction of mixed Mn–Zr oxides: in situ XPS and XRD studies, Dalton Trans. 44 (35) (2015) 15499–15507.

[49] X. Gu, J. Yue, L. Chen, S. Liu, H. Xu, J. Yang, Y. Qian, X. Zhao, Coaxial MnO/N-doped carbon nanorods for advanced lithium-ion battery anodes, J. Mater. Chem. 3 (3) (2015) 1037–1041.

[50] M.C. Biesinger, B.P. Payne, A.P. Grosvenor, L.W. Lau, A.R. Gerson, R.S.C. Smart, Resolving surface chemical states in XPS analysis of first row transition metals, oxides and hydroxides: Cr, Mn, Fe, Co and Ni, Appl. Surf. Sci. 257 (7) (2011) 2717–2730.

[51] H. Lv, H. Zhao, T. Cao, L. Qian, Y. Wang, G. Zhao, Efficient degradation of high concentration azo-dye wastewater by heterogeneous Fenton process with iron-based metal-organic framework, J. Mol. Catal. Chem. 400 (2015) 81–89.

[52] Z.-J. Jiang, Z. Jiang, Interaction induced high catalytic activities of CoO nanoparticles grown on nitrogen-doped hollow graphene microspheres for oxygen reduction and evolution reactions, Sci. Rep. 6 (2016) 27081.

[53] L. Lukashuk, N. Yigit, H. Li, J. Bernardi, K. Föttinger, G. Rupprechter, Operando XAS and NAP-XPS investigation of CO oxidation on meso-and nanoscale CoO catalysts, Catal. Today 336 (2019) 139–147.

[54] P. Mondal, A. Sinha, N. Salam, A.S. Roy, N.R. Jana, S. Islam, Enhanced catalytic performance by copper nanoparticle–graphene based composite, RSC Adv. 3 (16) (2013) 5615–5623.

[55] Y. Bao, K. Chen, $AgCl/Ag/g\text{-}C_3N_4$ hybrid composites: preparation, visible light-driven photocatalytic activity and mechanism, Nano-Micro Lett. 8 (2) (2016) 182–192.

[56] M.F. Bekheet, L. Dubrovinsky, A. Gurlo, Compressibility and structural stability of spinel-type $MnIn_2O_4$, J. Solid State Chem. 230 (2015) 301–308.

[57] M.F. Bekheet, L. Schlicker, A. Doran, K. Siemensmeyer, A. Gurlo, Ferrimagnetism in manganese-rich gallium and aluminium spinels due to mixed valence Mn^{2+}–Mn^{3+} states, Dalton Trans. 47 (8) (2018) 2727–2738.

[58] J. Yuan, S. Hapis, H. Breitzke, Y. Xu, C. Fasel, H.-J. Kleebe, G. Buntkowsky, R. Riedel, E. Ionescu, Single-source-precursor synthesis of hafnium-containing ultrahigh-temperature ceramic nanocomposites (UHTC-NCs), Inorg. Chem. 53 (19) (2014) 10443–10455.

[59] N. Anacleto, O. Ostrovski, S. Ganguly, Reduction of manganese oxides by methane-containing gas, ISIJ Int. 44 (9) (2004) 1480–1487.

[60] H. Cheng, Y. Li, E. Kroke, S. Herkenhoff, In situ synthesis of Si_2N_2O/Si_3N_4 composite ceramics using polysilyloxycarbodiimide precursors, J. Eur. Ceram. Soc. 33 (11) (2013) 2181–2189.

[61] R.M. Morcos, A. Navrotsky, T. Varga, D. Ahn, A. Saha, F. Poli, K. Müller, R. Raj, Thermodynamically stable $Si_wC_xN_yO_z$ polymer-like, amorphous ceramics made from organic precursors, J. Am. Ceram. Soc. 91 (7) (2008) 2391–2393.

[62] E. Ionescu, C. Terzioglu, C. Linck, J. Kaspar, A. Navrotsky, R. Riedel, Thermodynamic control of phase composition and crystallization of metal-modified silicon oxycarbides, J. Am. Ceram. Soc. 96 (6) (2013) 1899–1903.

[63] C. Vakifahmetoglu, E. Pippel, J. Woltersdorf, P. Colombo, Growth of one-dimensional nanostructures in porous polymer-derived ceramics by catalyst-assisted pyrolysis. Part I: iron catalyst, J. Am. Ceram. Soc. 93 (4) (2010) 959–968.

[64] M. Hojamberdiev, R.M. Prasad, C. Fasel, R. Riedel, E. Ionescu, Single-source-precursor synthesis of soft magnetic Fe_3Si and Fe_5Si_3-containing SiOC ceramic nanocomposites, J. Eur. Ceram. Soc. 33 (13–14) (2013) 2465–2472.

[65] R. Olesinski, G. Abbaschian, The Cu−Si (Copper-Silicon) system, Bull. Alloy Phase Diagrams 7 (2) (1986) 170–178.

[66] R. Olesinski, G. Abbaschian, The Si-Zn (Silicon-Zinc) system, Bull. Alloy Phase Diagrams 6 (6) (1985) 545–548.

[67] R. Olesinski, A. Gokhale, G. Abbaschian, The Ag-Si (silver-silicon) system, J. Phase Equil. 10 (6) (1989) 635–640.